PAPER • **OPEN ACCESS**

Stemless InSb nanowire networks and nanoflakes grown on InP

To cite this article: Marco Rossi *et al* 2024 *Nanotechnology* **35** 415602

OPEN ACCESS
IOP Publishing
Nanotechnology

Nanotechnology **35** (2024) 415602 (10pp)
https://doi.org/10.1088/1361-6528/ad61ef

Stemless InSb nanowire networks and nanoflakes grown on InP

Marco Rossi[1], Teun A J van Schijndel[1,2], Pim Lueb[1], Ghada Badawy[1], Jason Jung[1], Wouter H J Peeters[1], Sebastian Kölling[3], Oussama Moutanabbir[3], Marcel A Verheijen[1,4] and Erik P A M Bakkers[1,*]

[1] Applied Physics and Science Education Department, Eindhoven University of Technology, 5600 MB, Eindhoven, The Netherlands
[2] Electrical and Computer Engineering, University of California Santa Barbara, Santa Barbara, CA 93106, United States of America
[3] Department of Engineering Physics, École Polytechnique de Montréal, Montreal, Québec, Canada
[4] Eurofins Materials Science Netherlands B.V., High Tech Campus 11, 5656 AE, Eindhoven, The Netherlands

E-mail: e.p.a.m.bakkers@tue.nl

Received 25 March 2024, revised 12 June 2024
Accepted for publication 11 July 2024
Published 24 July 2024

Abstract

Among the experimental realization of fault-tolerant topological circuits are interconnecting nanowires with minimal disorder. Out-of-plane indium antimonide (InSb) nanowire networks formed by merging are potential candidates. Yet, their growth requires a foreign material stem usually made of InP–InAs. This stem imposes limitations, which include restricting the size of the nanowire network, inducing disorder through grain boundaries and impurity incorporation. Here, we omit the stem allowing for the growth of stemless InSb nanowire networks on an InP substrate. To enable the growth without the stem, we show that a preconditioning step using arsine (AsH_3) is required before InSb growth. High-yield of stemless nanowire growth is achieved by patterning the substrate with a selective-area mask with nanohole cavities, containing restricted gold droplets from which nanowires originate. Interestingly, these nanowires are bent, posing challenges for the synthesis of interconnecting nanowire networks due to merging failure. We attribute this bending to the non-homogeneous incorporation of arsenic impurities in the InSb nanowires and the interposed lattice-mismatch. By tuning the growth parameters, we can mitigate the bending, yielding large and single crystalline InSb nanowire networks and nanoflakes. The improved size and crystal quality of these nanostructures broaden the potential of this technique for fabricating advanced quantum devices.

Supplementary material for this article is available online

Keywords: nanowires, metal organic vapor phase epitaxy, InSb, bending, nanoflakes

* Author to whom any correspondence should be addressed.

1. Introduction

Indium antimonide (InSb) is a semiconductor with ideal properties for quantum applications. Its high mobility, strong spin–orbit coupling, and Landé g-factor make it suitable for studying quantum phenomena in semiconductor–superconductor device hybrids based on nanowires [1–5]. These device hybrids have gained attention for their potential to host Majorana-zero-modes (MZMs), vital for enabling fault-tolerant topological quantum computation [6–8]. However, detecting MZMs experimentally has proven to be challenging due to material disorder [9–13], thus their existence remains an open question.

One method to demonstrate the existence of MZMs is by showcasing their non-abelian statistics through controlled braiding, requiring a complex network of interconnecting nanowires with a selectively deposited superconductor [14–16]. Interconnecting out-of-plane InSb nanowire networks, grown on indium phosphide (InP) or indium arsenide (InAs) intermediary stems via the gold (Au) catalyzed vapor–liquid–solid (VLS) method, are promising infrastructures for these experiments [17–19], with reports of ballistic transport in this system [20, 21]. Nanowire interconnection between out-of-plane nanowires was realized by changing the growth direction during stem growth [17, 18] or by growing non-parallel stems on the inclined {111} facets of a (100) InP or InAs substrate [19, 21]. Moreover, the use of stems facilitates InSb nanowire growth as the direct nucleation of InSb nanowires on the substrate is challenging due to the surfactant effect of antimony (Sb) [22, 23], which causes the Au droplet to be propelled on the surface rather than promoting vertical nanowire growth [24]. Nonetheless, stems give rise to problems for MZMs experiments. The mixed-crystal-phase nature of the stems induces disorder in interconnecting InSb nanowires causing the formation of grain boundaries [17, 18, 25] (see figure S1(a) in the supplementary information) or lead to arsenic (As) or phosphorous (P) impurity incorporation [24, 26]. Moreover, they restrict the overall extension of the semiconductor–superconductor device hybrid since stems evaporate during InSb growth [24, 27, 28], thereby limiting the InSb nanowire growth time and thus its length to approximately 3.5 μm (figure S1(b)). Larger nanowire networks are necessary to accommodate gate connections, multiple superconducting islands [29] and reduce wavefunction overlap among different MZMs [30] (figure S1(c)).

In this study, we present a method for achieving stemless InSb nanowires on InP adopting a preconditioning step with arsine (AsH_3) before InSb growth and by effectively confining the Au droplets using a selective-area mask fabricated on the growth substrate. However, nanowires grown using this method exhibit bending, which could hinder nanowire interconnection when growing out-of-plane networks. To address this issue, we conducted a comprehensive investigation including statistical analysis, material characterization and modeling to identify the causes of bending and explore mitigation strategies. We explain the origin of the bending, rooted in the prior use of AsH_3 in the growth chamber, and resulting from the non-homogeneous incorporation of As impurities in the nanowires following an asymmetrical core–shell scheme, causing lattice mismatch. Armed with this improved understanding of bending, we successfully mitigated it by tuning the growth parameters, achieving single-crystalline stemless nanowire networks and nanoflakes, surpassing their stemmed counterparts in length, reaching sizes of tens of microns.

2. Methods

InP(111)B (for vertical nanowire growth) and InP(100) substrates with etched V-grooves (for interconnecting nanowire growth, as reported at [25]) have been prepared for nanowire growth. The fabrication of the amorphous selective-area silicon nitride (SiN_x) mask with nanoholes on both these substrates starts by depositing a 20 nm thin layer of SiN_x on the substrate using plasma-enhanced physical vapor deposition. A positive resist is spun on the substrate and circular nanoholes with varying pitch are then patterned using electron-beam-lithography. After resist development, two methods for nanohole fabrication within the SiN_x mask are tested: one set of samples undergoes a dry etching process utilizing a reactive-ion etching tool, while another set undergoes wet etching using a buffered hydrofluoric acid solution. A 8 nm thin layer of Au is deposited on both sets of samples by electron-beam physical vapor deposition, followed by resist lift-off, leaving Au only in the nanoholes. Dry-etched nanoholes have parallel sidewalls, whose pattern is established by the lithography design, and contain Au droplets with a similar diameter (see figures S2(a), (c), (e)). On the other hand, wet-etched nanoholes have inclined sidewalls and are usually larger compared to the intended size of the lithography design due to the isotropic nature of the etching, resulting in Au droplets with a significantly smaller diameter than the nanoholes (see figures S2(b), (d), (f)). The detailed fabrication recipe of the substrate can be found in section SI.1 of the supplementary information.

The InSb nanowire growth is performed in a horizontal Aixtron MOVPE reactor, using molecular hydrogen as carrier gas for the precursors, which are trimethylantimony (TMSb) and trimethylindium (TMIn). The InSb growth is preceded by a heating-up step using either TMSb, or an alternative group-V precursor, namely phosphine (PH_3) or AsH_3. The growth scheme used to test the nanowire growth using the PH_3 or AsH_3 heat-up steps is sketched in figure 1(b). In case of PH_3 or AsH_3 heat-up, InSb growth is started only for 30 s ('nucleation' step) and followed by a step in which the reactor is flushed with TMSb for 2 min to remove any PH_3 or AsH_3 residuals. Subsequently, InSb growth is performed for 90 min. The growth with a TMSb heat up step follows a similar growth scheme developed in a previous work on the homoepitaxial growth of InSb nanowires [24]. The growth runs using different group-V species during heating-up are performed in separate reactors to avoid cross-contamination, and this is achieved by replacing the quartz reactor walls and substrate susceptor between different runs. The samples are kept under constant rotation during the whole duration of the growth scheme. Additional growth details can be found in section SI.1 of the supplementary information.

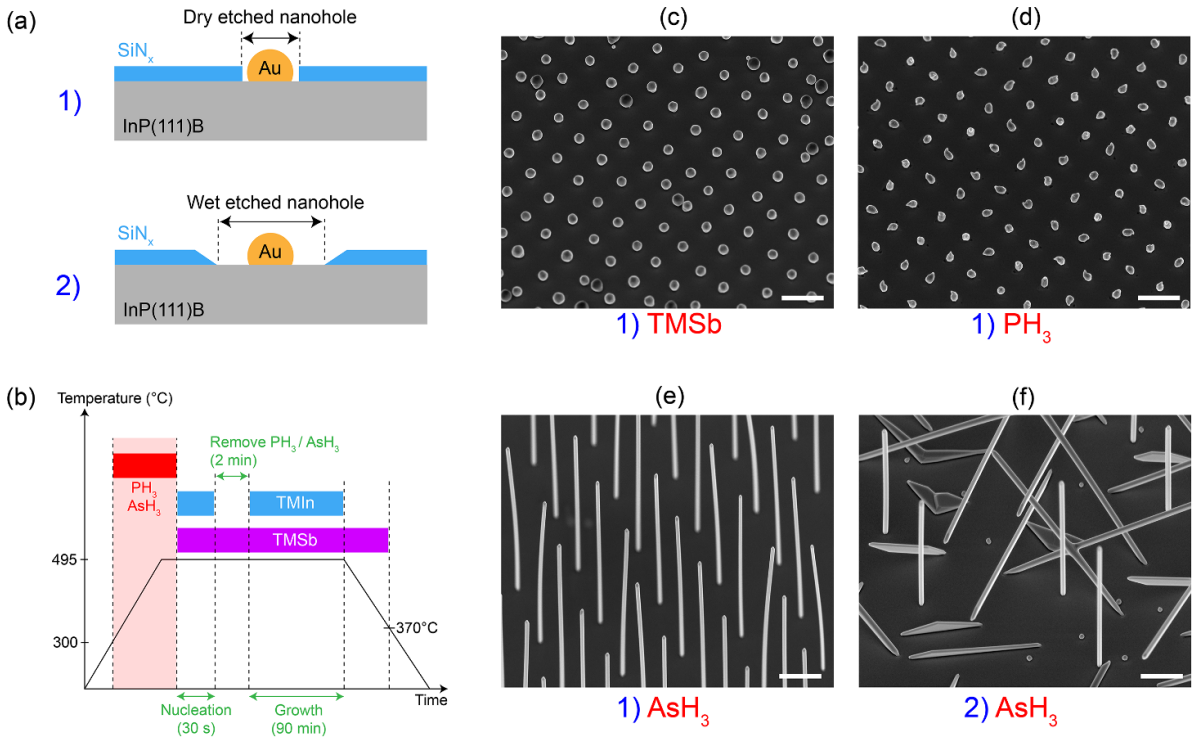

Figure 1. (a) Sketches of the substrates for nanowire growth. Au droplets are confined within SiN_x nanoholes defined by lithography and etched with dry or wet etching, which yield two different cavity shapes. (b) Sketch of the MOVPE growth scheme used to test the stemless InSb nanowire growth. (c)–(f) Representative side view SEM images of the growth outcomes using the substrates shown in (a) and different group-V species during heat-up. (c) Heat-up under TMSb and dry-etched nanoholes (growth scheme of [24]). (d), (e) Dry-etched nanoholes and heat-up under PH_3 and AsH_3, respectively, using the growth scheme shown in (b). (f) Wet-etched nanoholes and heat-up under AsH_3, using the growth scheme shown in (b). Scale bars are 1 μm. Pictures (c)–(f) were taken with the SEM stage tilted by 30°.

3. Results and discussion

The goal of this work is to develop advanced self-shadowing nanowire network structures for novel semiconductor–superconductor quantum devices based on InSb nanowires. To achieve this, an InP(100) platform with etched V-grooves, as developed in previous studies [19, 25, 31], will be utilized for growing such nanostructures. In these previous works, tilted InSb nanowires have been grown using InAs/InP stem nanowires on the {111}B-sloped facets. In this work we want to develop a process to grow InSb nanowires on InP substrates without using a stem to be able to grow much longer InSb nanowires [24]. We therefore start this work with developing the growth on planar InP(111)B substrates and in the last part of the manuscript we discuss growth in the V-grooves, consisting of {111}B facets in a (100) wafer. For the growth of InSb nanowires on InP(111)B we first study the effect of the shape of the nanohole cavity in the SiN_x mask and the preconditioning step on the InSb nanowire growth. The two different nanohole cavities are illustrated in figure 1(a), and are realized by two different fabrication processes (see methods section and section SI.1 of the supplementary information) and basically differ in the ratio of the Au-island size with respect to the nanohole opening size. This ratio is a very important parameter that influences the nucleation and growth of the nanowires, as shown in a previous study for the growth on InSb(111) substrates [24]. To study the effect of preconditioning, the samples have been exposed to TMSb, AsH_3 or PH_3 while the sample is heated up from 300 °C to 495 °C prior the growth, following the growth scheme of figure 1(b).

Figures 1(c)–(e) are representative scanning electron microscopy (SEM) images of the growth on samples with dry-etched nanoholes that underwent one of the three different preconditioning steps. Both the growth with TMSb and PH_3 heat-up steps show that InSb crystals have nucleated within each nanohole without leading to any vertical nanowire growth. On the other hand, the exposure to AsH_3 during heat-up leads to a high yield of long ($\sim$10 μm) vertical InSb nanowires having a thickness ranging from 85 to 115 nm depending on the pitch (figures 1(e) and S3). Transmission-electron-microscopy (TEM) reveals that these nanowires display a defect-free zincblende crystal structure and are grown via the Au-catalyzed VLS mode (see figure S11). The sample with wet-etched nanoholes, grown in the same run, displays a low yield of vertical nanowire growth (figures 1(f) and S3). In this case, most of the Au droplets seem to slide laterally once exceeded the height of the nanohole cavity, forming nanostructures that in some cases merge with neighboring ones. The SiN_x mask effectively suppresses the formation of parasitic InSb islands on the substrate in every growth run. From this study it is evident that As-exposure during heating up is essential to initiate the growth of InSb nanowires, otherwise they do not nucleate. Furthermore, the small nanohole cavities result in a high yield of vertical InSb nanowires, which is

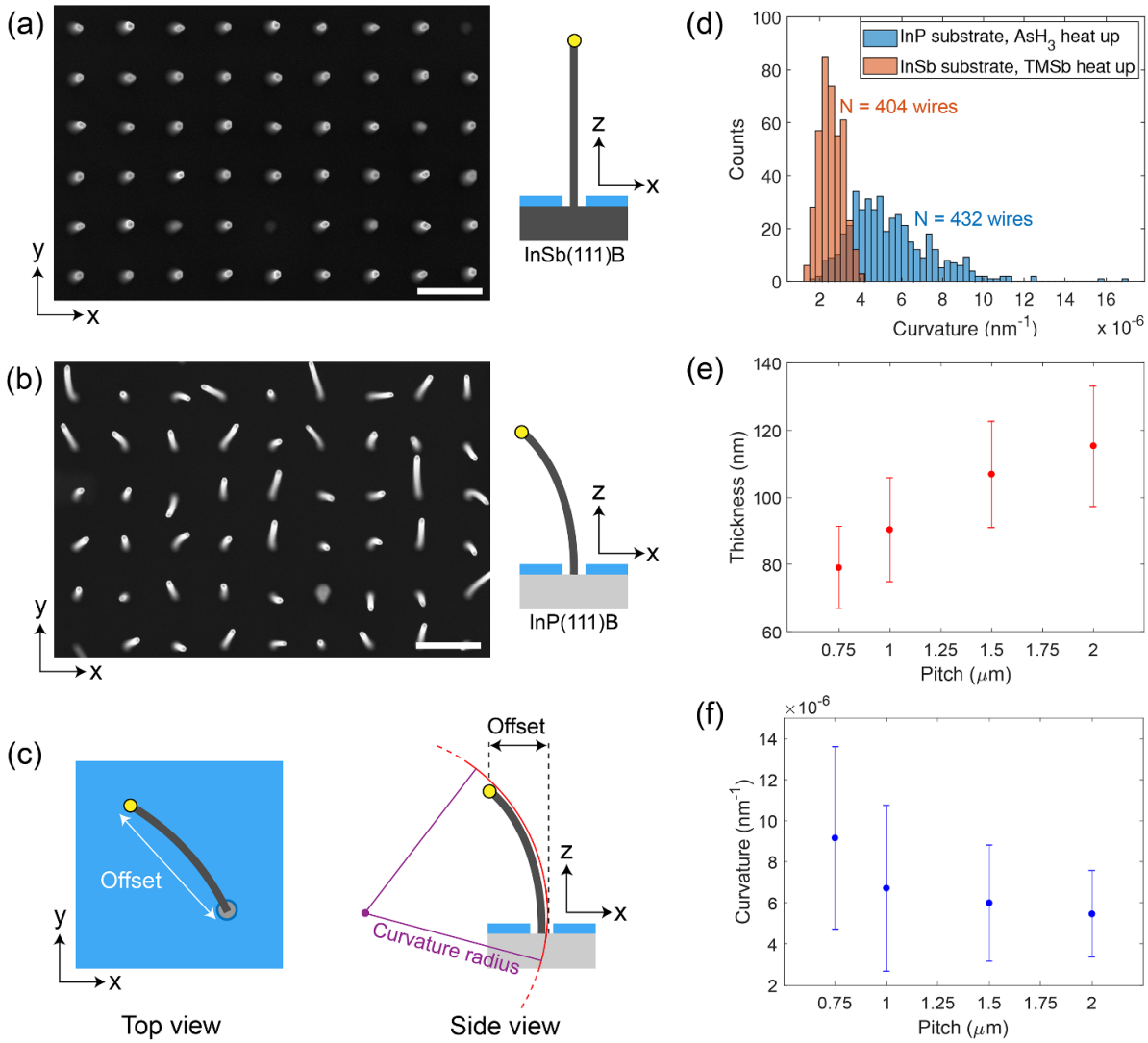

Figure 2. (a) Representative SEM top-view image of the stemless nanowires grown on InSb without employing AsH_3 and in an As-free reactor, and a sketch from the side view (b) representative SEM top-view image of the stemless nanowires grown on InP using AsH_3 during heat-up, and a sketch from the side view. Scale bars are 1 μm. (c) Top-view and side-view sketches of a bent nanowire. The SEM image recognition software retrieves the 'offset' of each nanowire in an SEM top-view picture, which is used to estimate its curvature, i.e. the inverse of its curvature radius. (d) Comparison between the curvature distributions of a similar number (N) of stemless nanowires grown on InP using an AsH_3 heat-up (blue bins) and stemless nanowires grown on InSb using a TMSb heat-up (orange bins). (e), (f) Results of the statistical analysis of a sample of stemless InSb nanowires grown on InP from dry-etched nanoholes, displaying the (e) nanowire thickness and (f) nanowire curvature as a function of the pitch. Means and error bars of the curvature are calculated by fitting the curvature distributions of nanowire field with different pitch (see figure S9 of the supplementary information).

important for their use in the self-shadowing structures. We emphasize, however, that the InSb nanowires of which the growth has been initiated by AsH_3 preconditioning seem to be bent, especially the nanowires with the smaller diameters, which may affect the electronic properties [32, 33].

Therefore, we next investigate and quantify the bending of the InSb nanowires. As a reference sample, stemless InSb nanowires are grown on InSb(111)B substrates with a patterned SiN_x mask with dry-etched nanoholes. Growth is performed without using AsH_3 and in an As-free reactor (growth details can be found here [24]). The resulting nanowires appear straight from the top-view SEM image (figure 2(a)), in contrast to the InSb wires grown on InP(111) by using AsH_3 (figure 2(b)). The curvature of the nanowires grown on these two substrates is determined from a statistically relevant number of nanowires (>400) using SEM image-recognition software (see section SI.2 of the supplementary information for details). The software analyzes both top-view and side-view SEM images of nanowire fields and extracts geometric information of each nanowire, e.g. nanowire thickness and length. To estimate the level of bending of nanowires, the software measures the 'offset' between base and tip of the nanowire when

viewed from top-view as illustrated in figure 2(c). Figure 2(d) compares the curvature distributions of InSb nanowires grown on InSb (orange) and InP (blue) substrates. Nanowires grown on InSb (in an As-free reactor) are all apparently 'curved' in the same direction, which can be explained by imperfect sample clamping prior SEM imaging (see figure S8 and section SI.2). The imperfect clamping procedure results in a consistent systematic error in the offset, leading to an apparent nanowire curvature, that we quantify at 2.7×10^{-6} nm^{-1}. In contrast, nanowires grown on InP substrates with an AsH_3 preconditioning step display a significantly broader curvature distribution, with nanowires exhibiting curvatures even an order of magnitude greater than the systematic error (see figure S9). Therefore, the presence of this systematic error has a minimal impact on the determination of mean curvatures and spreads of nanowires grown using AsH_3. The study of the bending orientation of nanowires grown using AsH_3 reveals that they can be bent in every direction, although a preferential bending orientation seems to exist (see figure S9 and section SI.2). The underlying causes of this preferential orientation, which we do not further explore, remains unknown.

The influence of the pitch on the aspect ratio and bending is studied and the results of the analysis of a representative sample are shown in figures 2(e) and (f), highlighting that nanowire thickness and curvature exhibit opposite monotonic behavior, with the thickness increasing and curvature decreasing as a function of the pitch. The nanowire length is unaffected by the pitch (see figure S7). The thickness increase for larger pitch suggests a contribution of surface diffusion of growth units from the mask towards the side-facets of the nanowires. The opposite behavior of thickness and curvature suggests that thicker wires are stiffer and thus bend less.

To explain the bending of the nanowires, a first hypothesis is to attribute it to the 10.4% lattice mismatch between InSb and InP [1, 2], which typically induces defects when growing blanket InSb layers on mismatched substrates [34–37]. Nanowires are known to better accommodate lattice mismatch due to their small footprints [38, 39], but elastic strain may occur to prevent the formation of threading dislocations [40]. However, we have evidence that strain due to lattice mismatch is fully relaxed at the InP–InSb nanowire interface (see figures S12(a)–(c)). A second hypothesis for the bending behavior could be the use of As during heat up, which might lead to the known 'carry-over' effect [41–45]. Arsenic can stick to the internal parts of the growth chamber and outgas at high temperatures during all the subsequent growth steps, thus being unintentionally incorporated into the growing nanowires and form an $InAs_xSb_{1-x}$ alloy. Considering that InSb and InAs have a lattice mismatch of about 7% [1, 2], the presence of As impurities with varying concentration within the InSb nanowires can lead to strain, and thus bending. This hypothesis is tested by employing the AsH_3 preconditioning on a InSb(111)B sample for nanowire growth. Interestingly, the resulting nanowires exhibit the same bending as those grown on an InP(111)B substrate (see figure S4), supporting the As carry-over hypothesis.

We perform cross-sectional scanning-transmission electron microscopy-energy dispersive x-ray spectroscopy (STEM-EDX) analysis to check the presence of As impurities in the nanowires grown using AsH_3 during preconditioning. Ten nanowires are transferred from the InP growth substrate to a bare wafer. Subsequently, cross-sectional TEM lamellas are created including all ten wires using a focused-ion beam; note that each wire is cut at a specific height from their base (see figure S13). The presence of As impurities is detected in all the nanowires under study, proving the occurrence of the As carry-over effect. Out of ten nanowires, eight nanowires (A1–C1 and A2–E2 in figure S13) possess two common characteristics, that can be visualized in the representative STEM-EDX cross-sectional cut shown in figure 3(a). First, the nanowires display a distorted hexagonal cross-section due to unequally long {110} side facets. Second, As is unevenly distributed within the nanowire cross-section forming an As-poor core surrounded by an As-rich shell with varying As fractions. The difference in As molar fraction between core and shell ranges from $x = 0.039$ to $x = 0.086$ and leads to an approximately 0.3% variation in lattice parameter of the $InAs_xSb_{1-x}$ alloy [46]. The combination of these two characteristics results in an asymmetrical core–shell distribution of the lattice parameter, which is known to cause bending in nanowires [47–63]. We note that the As-poor core area is similar among the eight nanowires, while the thickness of the As-rich shell varies and seems to be connected to the pitch of the field from which the nanowires were transferred. We interpret the As-poor core area as the volume realized by the vertical Au-catalyzed VLS-growth and the As-rich outer shell as the radial, vapor-solid (VS) grown part. Possibly, these two growth modes have different As incorporation efficiencies. The other two remaining sectioned nanowires (D1 and E1 in figure S13) display a distorted hexagonal cross-section and uneven As incorporation, but seem to not conform to the core–shell scheme.

We verify the presence of As impurities along the length of nanowires grown with the AsH_3 preconditioning by performing atom-probe-tomography (APT) on a bent nanowire (see figure S14). Results show that As is present along the entire length of the nanowire, with an average As fraction in the probed volume ranging from $x = 0.06$ near the base to 0.04 towards the tip. These values are consistent with the As molar fractions measured by STEM-EDX (see figure S14). The slight decrease of As fraction along the nanowire could be due to the consumption of residual As overtime from the growth chamber.

A bending model is devised to gain a deeper understanding of nanowire bending and explain the results of the statistical analysis. The STEM-EDX cross-sectional study provides the basis for our model and serves as a source of input parameters (see figure S13). The APT study is not considered as a source of input parameters because the probed volume of the nanowire with this technique is too narrow to image the distribution of atomic species in the entire nanowire cross-sectional plane (see figure S14). Therefore, only the STEM-EDX cross-sectional study is used for constructing the bending

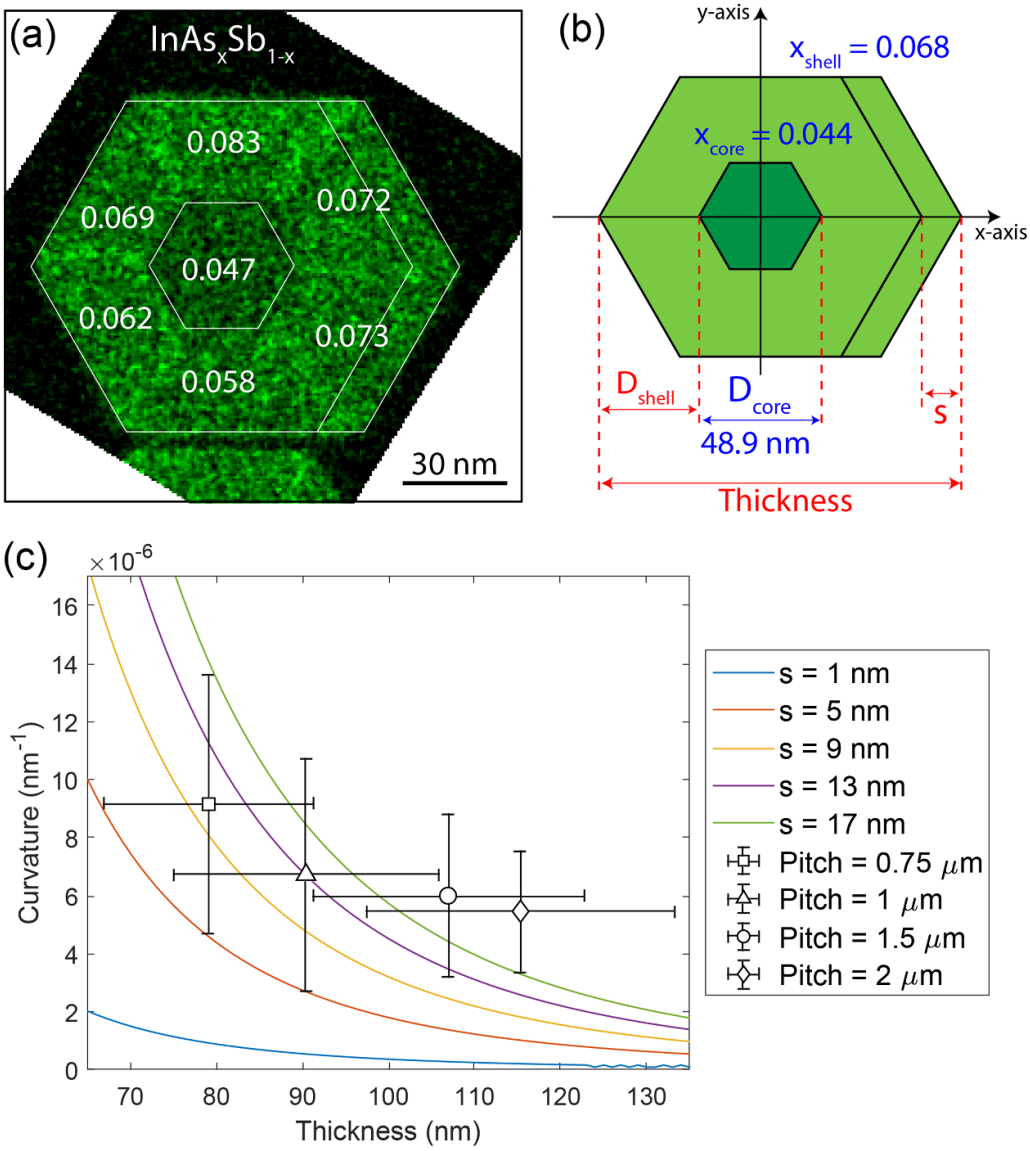

Figure 3. A representative As map from a STEM-EDX cross-sectional sample of a stemless InSb nanowire grown on InP using AsH_3 during heat-up. The quantified As molar fractions ('x') in different parts of the cross-section are displayed. The accuracy in percentage As for areas selected within the STEM-EDX mapping is approximately 0.5 at%. Thus, the As molar fraction has an error of ∼0.008. The nanowire has an As-poor core surrounded by an asymmetric As-rich shell, with varying As molar fractions, outlined by the white lines. (b) Sketch of the nanowire cross-section used for the bending model, displaying the As molar fraction distribution, and input parameters. The nanowire is modeled as an $InAs_xSb_{1-x}$ alloy with a hexagonal asymmetric core–shell As distribution constant along the entire nanowire length. As molar fractions in the core and shell are considered homogeneous. The asymmetry in the hexagonal shape is modeled with a thickening 's' of the nanowire shell along two adjacent {110} side facets. The input parameters of the model are the core thickness (D_{core}), the As core molar fraction (x_{core}), and the As shell molar fraction (x_{shell}). The nanowire thickness is defined as the sum of D_{core}, s, and twice the shell thickness (D_{shell}). (c) Comparison between the calculated nanowire curvatures as a function of thickness resulting from the bending model, for different values of s, and the results of the statistical analysis of figures 2(e) and (f).

model. The nanowire cross-section is modeled as an asymmetric core–shell structure, uniform along the entire length of the nanowire, and is depicted in figure 3(b). The core and asymmetric shell are both considered homogeneous and composed of an $InAs_xSb_{1-x}$ alloy, with two different As fractions and lattice constants correlated by Vegard's law [46]. The shell thickness D_{shell} is considered a variable, while the extent of the As-poor core area, given by the parameter D_{core}, is considered constant and equal to the average diameter measured among the sectioned nanowires. The asymmetry of the structure is modeled by introducing a thickening, s, of two adjacent {110} side facets, having the same As fraction of the shell. By iterating over a range of D_{shell} and s, the model calculates the nanowire curvature as a function of thickness resulting from the lattice mismatch. For further details on the bending model, see section SI.3 of the supplementary information.

Figure 3(c) displays the bending model results for several asymmetric thickening s and compares them to the statistical analysis results of figures 2(e) and (f). The range of s extends up to $s = 17$ nm, which is the largest observed

value in the STEM-EDX cross-sectional study. The experimental data and theoretical predictions show a similar trend and curvature order of magnitude, but deviations occur for thicker nanowires. These deviations can be attributed to the complex nature of the grown nanowires, which exhibit various distorted hexagonal shapes, variations in As fraction within the shell, and likely a variation in As incorporation along the nanowire. Additionally, the occurrence of the systematic error prior to SEM imaging, although causing minor changes to the curvature distributions and mean values, should be considered when comparing experimental and theoretical data. Overall, the bending model is in good agreement with the experimental results and captures the physics of nanowire bending in this system. The results of the model show that bending can be mitigated growing a thicker shell around the core, and this can be achieved by enhancing the VS InSb growth on the nanowire sidewalls by increasing the pitch.

The understanding of the stemless InSb nanowire growth using an AsH_3 heat up is applied to grow complex nanowire networks and nanoflakes on a InP(100) platform with inclined {111}B facets, named trenches (see [25] for platform fabrication details). Dry etching is used to fabricate the nanoholes in the SiN_x mask. A schematic illustration of the platform for nanowire growth is shown in figure 4(a). Different InSb nanostructures can be grown in pre-determined positions and orientations by tuning the offset (Δy in figure 4(a)) of pairs of Au particles deposited on opposing facets of neighboring trenches. We adopt a large nanowire inter-distance along the trenches to favor the VS InSb growth on the nanowire sidewalls, which minimizes the bending and ensures that each nanowire interconnects with others with the intended Δy (figures 4(b) and S5). Stemless InSb nanowire and nanoflakes grown in this way display a thickness within the 120–180 nm range.

The stemless growth grants several benefits for the fabrication of complex semiconductor–superconductor device hybrids compared to stemmed nanowire growth. By tuning the growth time, stemless nanowires can interconnect with each other up to lengths of tens of microns, enabling the fabrication of larger nanowire networks (>6.5 μm, figure 4(c)) or nanoflakes (>12 μm^2, figure 4(d)) compared to stemmed ones that suffer from stem evaporation (~3.5 μm and ~2 μm^2, respectively) [24, 25]. The increased length broadens the design possibilities of superconductor-semiconductor hybrid devices, exploiting the smart inter-shadowing effect between neighboring nanostructures during the directional superconductor deposition. This selective superconductor deposition mitigates the need for potentially detrimental post-fabrication steps that could affect the quality of the devices, ensuring smooth and pristine interfaces [64–67]. Moreover, stem omission ensures that all the interconnecting nanowires are epitaxially connected to the substrate and thus merge without forming grain boundaries, as indicated by the trapezoidal morphology of all the final nanoflakes or nanobridges (see figures 4(b), (d) and

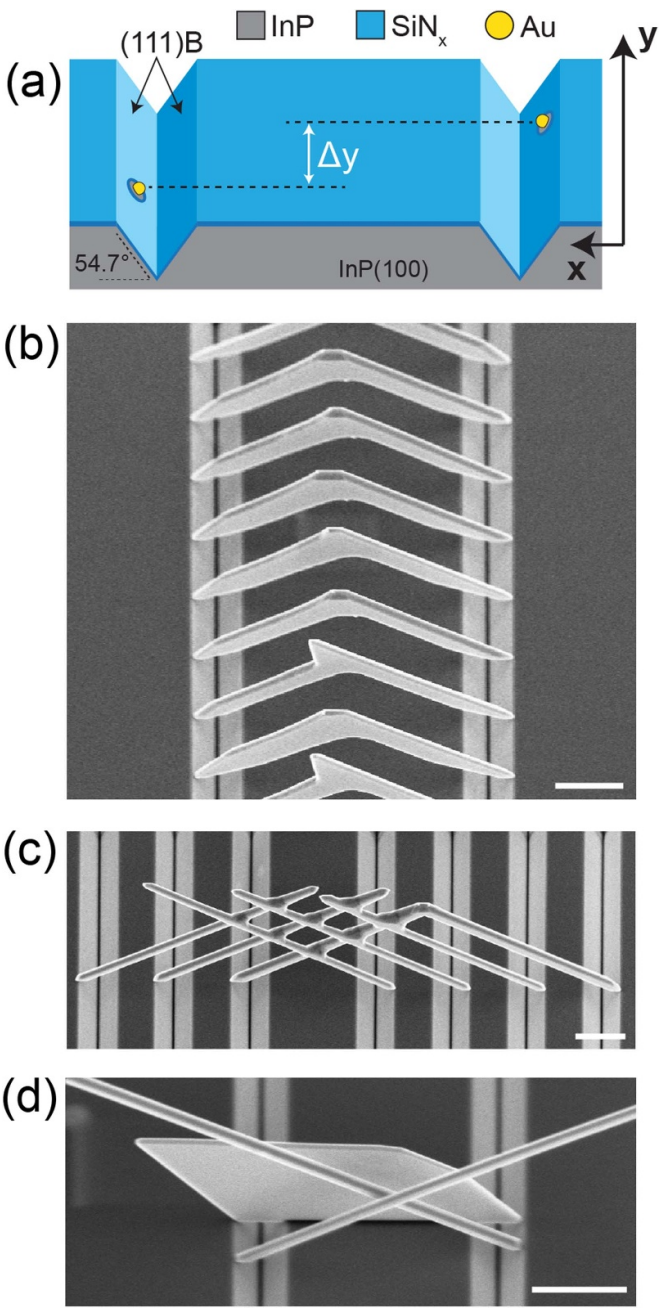

Figure 4. (a) Sketch of the platform for creating a wide variety of designs of InSb nanowire networks or nanoflakes. Control over the nanowire direction is achieved by patterning inclined InP{111}B facets ('trenches') with Au droplets at specific locations on the substrate. Nanowire interconnection can be controlled by adjusting the offset (Δy) of pairs of Au droplets deposited on opposing facets of neighboring trenches, allowing for the fabrication of nanoflakes ($\Delta y = 0$), interconnecting nanowires ($\Delta y \sim t/2$, where t is the nanowire thickness), and standing nanowires ($\Delta y > t$). (b)–(d) Representative side-view SEM images of stemless InSb nanostructures grown on the platform. (b) A series of intentionally grown InSb nanoflakes in the early stages of growth, highlighting a high yield of perfectly merged nanowires. (c) An example of a large hashtag nanowire network, and (d) a nanoflake. Scale bars are all 1 μm.

S5), a hallmark of the absence of grain or twin boundaries [25]. All the nanoflakes analyzed by TEM are single-crystalline.

4. Conclusion and outlook

In summary, we achieved the growth of stemless InSb nanowires on InP by patterning the substrate with Au droplets, restricting them with a selective-area mask and exposing them to AsH_3 before InSb growth. The confinement of the Au droplets within narrow nanohole cavities of the mask is crucial to ensure a high yield of vertical nanowire growth. We demonstrate that the use of AsH_3 prior InSb nanowire growth contaminates our growth chamber, resulting in a continuous incorporation of a small percentage of As impurities throughout the 90 min of the InSb growth ('As carry-over'). As impurities are unevenly incorporated in the VLS-grown core and the VS-grown shell of the nanowires. The variations in shell thickness and As content lead to an asymmetric $InAs_xSb_{1-x}$ core–shell system with varying lattice parameter within the core/shell cross-sectional plane, leading to nanowire bending. We grow single-crystalline, long, stemless InSb nanowire networks and nanoflakes on an InP substrate with inclined {111}B facets by adopting growth conditions that enhance the VS growth on the nanowire sidewalls, yielding thicker and straighter nanowires. This method surpasses previous growth schemes based on stems for the fabrication of semiconductor–superconductor device hybrids through shadowing superconductor deposition, broadening the potential of this technique.

However, this work also highlights the drawbacks of using an As species to help nucleating InSb nanowires, as disorder is induced in the nanowires due to the As carry-over. A workaround could be to use short, As-contaminated InSb nanowires as stems for a following InSb growth performed in another As-free reactor or using molecular beam epitaxy (MBE), although the feasibility of this technique needs to be tested. Full MBE growth of stemless InSb nanowires could also be explored, using an As Cracker as the As source to initiate the InSb nanowire growth, and subsequently closing the As shutter to continue the growth of pure InSb nanowires from indium and antimony elemental sources. Nonetheless, it might still be challenging to completely eliminate the presence of As carry-over with this method, as reported in a prior study [45]. Alternatively, developing InSb platforms with inclined {111}B facets such as trenches or ridges, similar to those developed on InP [19, 25, 68] or InAs [21, 65], could eliminate the need for As or stems to initiate InSb nanowire nucleation [24].

Data availability statement

The data that support the findings of this study are openly available at the following URL/DOI: 10.5281/zenodo.10868471.

Acknowledgments

The authors thank René van Veldhoven for the support with the MOVPE reactor at the Eindhoven University of Technology. The authors thank NanoLab@TU/e and all the cleanroom personnel for their help and support. This work was supported by the European Research Council (ERC TOCINA 834290), and the Dutch Organization for Scientific Research (NWO). The authors acknowledge Solliance, a solar energy R&D initiative of ECN, TNO, Holst, TU/e, imec and Forschungszentrum Jülich, and the Dutch province of Noord-Brabant for funding the TEM facility. APT work was supported by NSERC Canada, Canada Research Chairs, and Canada Foundation for Innovation.

Author contributions

M R and T A J S contributed equally to this work. T A J S carried out the substrate fabrication and nanowire growth, M R and G B supported. P L developed the SEM image-recognition software ('APIMs') utilized for the statistical analysis of nanowire bending. M R, T A J S and G B performed the statistical analysis of nanowire bending, P L supported. M R and T A J S transferred nanowires for T E M J J and W H J P made FIB cuts for the TEM analysis. M A V performed the TEM analysis. S K performed the atom-probe tomography study under the supervision of O M, T A J S developed the bending model. M R carried out the comparison between statistical analysis, TEM data and bending model prediction. M A V and E P A M B provided key suggestions and discussions and supervised the project. M R wrote the manuscript with input from all the co-authors.

ORCID iDs

Marco Rossi https://orcid.org/0000-0002-2801-7790
Oussama Moutanabbir https://orcid.org/0000-0002-0721-3696
Marcel A Verheijen https://orcid.org/0000-0002-8749-7755
Erik P A M Bakkers https://orcid.org/0000-0002-8264-6862

References

[1] Madelung O 1991 *Semiconductors: Group IV Elements and III–V Compounds* (Springer) (https://doi.org/10.1016/0025-5408(91)90075-w)
[2] Vurgaftman I, Meyer J R and Ram-Mohan L R 2001 Band parameters for III–V compound semiconductors and their alloys *J. Appl. Phys.* **89** 5815–75
[3] Lutchyn R M, Sau J D and Das Sarma S 2010 Majorana fermions and a topological phase transition in semiconductor-superconductor heterostructures *Phys. Rev. Lett.* **105** 077001

[4] Oreg Y, Refael G and Von Oppen F 2010 Helical liquids and Majorana bound states in quantum wires *Phys. Rev. Lett.* **105** 177002

[5] Van Weperen I, Tarasinski B, Eeltink D, Pribiag V S, Plissard S R, Bakkers E P A M, Kouwenhoven L P and Wimmer M 2015 Spin-orbit interaction in InSb nanowires *Phys. Rev.* B **91** 201413

[6] Lutchyn R M, Bakkers E P A M, Kouwenhoven L P, Krogstrup P, Marcus C M and Oreg Y 2018 Majorana zero modes in superconductor-semiconductor heterostructures *Nat. Rev. Mater.* **3** 52–68

[7] Frolov S M, Manfra M J and Sau J D 2020 Topological superconductivity in hybrid devices *Nat. Phys.* **16** 718–24

[8] Das Sarma S 2023 In search of Majorana *Nat. Phys.* **19** 165–70

[9] Prada E, San-Jose P, de Moor M W A, Geresdi A, Lee E J H, Klinovaja J, Loss D, Nygård J, Aguado R and Kouwenhoven L P 2020 From Andreev to Majorana bound states in hybrid superconductor–semiconductor nanowires *Nat. Rev. Phys.* **2** 575–94

[10] Pan H and Das Sarma S 2020 Physical mechanisms for zero-bias conductance peaks in Majorana nanowires *Phys. Rev. Res.* **2** 013377

[11] Das Sarma S and Pan H 2021 Disorder-induced zero-bias peaks in Majorana nanowires *Phys. Rev.* B **103** 195158

[12] Ahn S, Pan H, Woods B, Stanescu T D and Das Sarma S 2021 Estimating disorder and its adverse effects in semiconductor Majorana nanowires *Phys. Rev. Mater.* **5** 124602

[13] Woods B D, Das Sarma S and Stanescu T D 2021 Charge-impurity effects in hybrid Majorana nanowires *Phys. Rev. Appl.* **16** 054053

[14] Aasen D *et al* 2016 Milestones toward Majorana-based quantum computing *Phys. Rev.* X **6** 031016

[15] Plugge S, Rasmussen A, Egger R and Flensberg K 2017 Majorana box qubits *New J. Phys.* **19** 012001

[16] Karzig T *et al* 2017 Scalable designs for quasiparticle-poisoning-protected topological quantum computation with Majorana zero modes *Phys. Rev.* B **95** 235305

[17] Plissard S R *et al* 2013 Formation and electronic properties of InSb nanocrosses *Nat. Nanotechnol.* **8** 859–64

[18] Car D, Wang J, Verheijen M A, Bakkers E P A M and Plissard S R 2014 Rationally designed single-crystalline nanowire networks *Adv. Mater.* **26** 4875–9

[19] Gazibegovic S 2019 Bottom-up grown InSb nanowire quantum devices *PhD Thesis* Eindhoven University of Technology

[20] Fadaly E M T, Zhang H, Conesa-Boj S, Car D, Gül Ö, Plissard S R, Op het Veld R L M, Kölling S, Kouwenhoven L P and Bakkers E P A M 2017 Observation of conductance quantization in InSb nanowire networks *Nano Lett.* **17** 6511–5

[21] Khan S A, Stampfer L, Mutas T, Kang J-H, Krogstrup P and Jespersen T S 2021 Multiterminal quantized conductance in InSb nanocrosses *Adv. Mater.* **33** 2100078

[22] Borg B M and Wernersson L 2013 Synthesis and properties of antimonide nanowires *Nanotechnology* **24** 202001

[23] Yuan X, Yang J, He J, Tan H H and Jagadish C 2018 Role of surface energy in nanowire growth *J. Phys. D: Appl. Phys.* **51** 283002

[24] Badawy G, Gazibegovic S, Borsoi F, Heedt S, Wang C-A, Koelling S, Verheijen M A, Kouwenhoven L P and Bakkers E P A M 2019 High mobility stemless InSb nanowires *Nano Lett.* **19** 3575–82

[25] Rossi M *et al* 2023 Merging nanowires and formation dynamics of bottom-up grown InSb nanoflakes *Adv. Funct. Mater.* **33** 2212029

[26] Caroff P, Wagner J B, Dick K A, Nilsson H A, Jeppsson M, Deppert K, Samuelson L, Wallenberg L R and Wernersson L-E 2008 High-quality InAs/InSb nanowire heterostructures grown by metal–organic vapor-phase epitaxy *Small* **4** 878–82

[27] Caroff P, Messing M E, Mattias Borg B, Dick K A, Deppert K and Wernersson L-E 2009 InSb heterostructure nanowires: MOVPE growth under extreme lattice mismatch *Nanotechnology* **20** 495606

[28] Plissard R, Slapak D R, Verheijen M A, Hocevar M, Immink G W G, van Weperen I, Nadj-Perge S, Frolov S M, Kouwenhoven L P and Bakkers E P A M 2012 From InSb nanowires to nanocubes: looking for the sweet spot *Nano Lett.* **12** 1794–8

[29] Stenger J P T, Woods B D, Frolov S M and Stanescu T D 2018 Control and detection of Majorana bound states in quantum dot arrays *Phys. Rev.* B **98** 085407

[30] Domínguez F, Cayao J, San-Jose P, Aguado R, Yeyati A L and Prada E 2017 Zero-energy pinning from interactions in Majorana nanowires *npj Quantum Mater.* **2** 13

[31] Op het Veld R L M 2021 InSANe InSb nanowire quantum devices *PhD Thesis* Eindhoven University of Technology

[32] Niquet Y M, Delerue C and Krzeminski C 2012 Effects of strain on the carrier mobility in silicon nanowires *Nano Lett.* **12** 3545–50

[33] Zeng L, Kanne T, Nygård J, Krogstrup P, Jäger W and Olsson E 2019 The effect of bending deformation on charge transport and electron effective mass of p-doped GaAs nanowires *Phys. Status Solidi* **13** 1900134

[34] Chyi J-I, Biswas D, Iyer S V, Kumar N S, Morkoç H, Bean R, Zanio K, Lee H-Y and Chen H 1989 Molecular beam epitaxial growth and characterization of InSb on Si *Appl. Phys. Lett.* **54** 1016–8

[35] Weng X, Goldman R S, Partin D L and Heremans J P 2000 Evolution of structural and electronic properties of highly mismatched InSb films *J. Appl. Phys.* **88** 6276–86

[36] Weng X, Rudawski N G, Wang P T, Goldman R S, Partin D L and Heremans J 2005 Effects of buffer layers on the structural and electronic properties of InSb films *J. Appl. Phys.* **97** 043713

[37] Tran T L, Hatami F, Masselink W T E D, Kunets V A S P and Salamo G J 2008 Comparison of MBE growth of InSb on Si (001) and GaAs (001) *J. Electron. Mater.* **37** 1799–805

[38] Kavanagh K L 2010 Misfit dislocations in nanowire heterostructures *Semicond. Sci. Technol.* **25** 024006

[39] Zhang X, Dubrovskii V G, Sibirev N V and Ren X 2011 Analytical study of elastic relaxation and plastic deformation in nanostructures on lattice mismatched substrates *Cryst. Growth Des.* **11** 5441–8

[40] Shin J C, Choi K J, Kim D Y, Choi W J and Li X 2012 Characteristics of strain-induced InxGa1−xAs nanowires grown on Si(111) substrates *Cryst. Growth Des.* **12** 2994–8

[41] Wada M, Seko M, Sakakibara K and Sekiguchi Y 1990 Incorporation of arsenic and gallium in InP layers in GaInAs/InP heterostructures grown by MOVPE *Jpn. J. Appl. Phys.* **29** 2342

[42] Keller B P, Brühl H G and Seifert W 1992 Carry-over—A fundamental problem in the MOVPE growth of heterostructures *Cryst. Res. Technol.* **27** 617–22

[43] Moon Y, Lee T, Yoon S, Yoo K and Yoon E 2000 Observation of two independent sources for arsenic carryover *J. Cryst. Growth* **208** 160–4

[44] Timò G, Calicchio M, Abagnale G, Armani N, Achilli E, Cornelli M, Annoni F, Schineller B and Andreani L C 2021 Study of the cross-influence between III–V and IV elements deposited in the same MOVPE growth chamber *Materials* **14** 1066

[45] Dudko I *et al* 2021 Hexagonal Ge grown by molecular beam epitaxy on self-assisted GaAs nanowires *Cryst. Growth Des.* **22** 32–36

[46] Denton A R and Ashcroft N W 1991 Vegard's "law" *Phys. Rev.* **43** 3161
[47] Hilse M, Takagaki Y, Herfort J, Ramsteiner M, Herrmann C, Breuer S, Geelhaar L and Riechert H 2009 Ferromagnet-semiconductor nanowire coaxial heterostructures grown by molecular-beam epitaxy *Appl. Phys. Lett.* **95** 133126
[48] Keplinger M, Kriegner D, Stangl J, Ma˚rtensson T, Mandl B, Wintersberger E and Bauer G 2010 Core-shell nanowires: from the ensemble to single-wire characterization *Nucl. Instrum. Methods Phys. Res.* B **268** 316–9
[49] Davtyan A *et al* 2020 X-ray diffraction reveals the amount of strain and homogeneity of extremely bent single nanowires *J. Appl. Crystallogr.* **53** 1310–20
[50] Yao X, Zhang X, Sun Q, Wei D, Chen P and Zou J 2021 Anomalous photoelectrical properties through strain engineering based on a single bent InAsSb nanowire *ACS Appl. Mater. Interfaces* **13** 5691–8
[51] Xu Y, Li L, Zang Y, Hu J, Li Z, Chen H, Zhang G, Xia C and Cho J-H 2021 Forward bending of silicon nanowires induced by strain distribution in asymmetric growth *Mater. Lett.* **297** 129929
[52] Al-humaidi M, Feigl L and Jakob J 2021 *In situ* x-ray analysis of misfit strain and curvature of bent polytypic GaAs–In x Ga1−x As core–shell nanowires *Nanotechnology* **33** 015601
[53] McDermott S and Lewis R B 2021 Bending of GaAs-InP core-shell nanowires by asymmetric shell deposition: implications for sensors *ACS Appl. Nano Mater.* **4** 10164–72
[54] Al Humaidi M *et al* 2023 Exploiting flux shadowing for strain and bending engineering in core-shell nanowires *Nanoscale* **15** 2254–61
[55] Mcdermott S, Smith T R, Lapierre R R and Lewis R B 2023 Phosphorus-controlled nanoepitaxy in the asymmetric growth of GaAs—InP Core—shell bent nanowires (arXiv:2305.07252)
[56] Krogstrup P, Ziino N L B, Chang W, Albrecht S M, Madsen M H, Johnson E, Nygård J, Marcus C and Jespersen T S 2015 Epitaxy of semiconductor -superconductor nanowires *Nat. Mater.* **14** 400–6
[57] Day R W, Mankin M N and Lieber C M 2016 Plateau-rayleigh crystal growth of nanowire heterostructures: strain-modified surface chemistry and morphological control in one, two, and three dimensions *Nano Lett.* **16** 2830–6
[58] Hetzl M, Winnerl J, Francaviglia L, Kraut M, Döblinger M, Matich S, Fontcuberta I Morral A and Stutzmann M 2017 Surface passivation and self-regulated shell growth in selective area-grown GaN-(Al,Ga)N core-shell nanowires *Nanoscale* **9** 7179–88
[59] Wallentin J, Jacobsson D, Osterhoff M, Borgström M T and Salditt T 2017 Bending and twisting lattice tilt in strained core-shell nanowires revealed by nanofocused x-ray diffraction *Nano Lett.* **17** 4143–50
[60] Lewis R B, Corfdir P, Küpers H, Flissikowski T, Brandt O and Geelhaar L 2018 Nanowires bending over backward from strain partitioning in asymmetric core-shell heterostructures *Nano Lett.* **18** 2343–50
[61] Gagliano L, Albani M, Verheijen M A, Bakkers E P A M and Miglio L 2018 Twofold origin of strain-induced bending in core-shell nanowires: the GaP/InGaP case *Nanotechnology* **29** 315703
[62] Bjergfelt M, Carrad D J and Kanne T 2019 Superconducting vanadium/indium-arsenide hybrid nanowires *Nanotechnology* **30** 294005
[63] Greenberg Y, Kelrich A, Cohen S, Kar-Narayan S, Ritter D and Calahorra Y 2019 Strain-mediated bending of InP nanowires through the growth of an asymmetric InAs shell *Nanomaterials* **9** 1327
[64] Carrad D J, Bjergfelt M, Kanne T, Aagesen M, Krizek F, Fiordaliso E M, Johnson E, Nygård J and Jespersen T S 2020 Shadow epitaxy for *in situ* growth of generic semiconductor/superconductor hybrids *Adv. Mater.* **32** 1908411
[65] Khan S A *et al* 2020 Highly transparent gatable superconducting shadow junctions *ACS Nano* **14** 14605–15
[66] Pendharkar M *et al* 2021 Parity-preserving and magnetic field—resilient superconductivity in InSb nanowires with Sn shells *Science* **372** 508–11
[67] Heedt S *et al* 2021 Shadow-wall lithography of ballistic superconductor–semiconductor quantum devices *Nat. Commun.* **12** 4914
[68] Dalacu D, Kam A, Austing D G and Poole P J 2013 Droplet dynamics in controlled InAs nanowire interconnections *Nano Lett.* **13** 2676–81